SPANDIDOS PUBLICATIONS

ONCOLOGY LETTERS 18: 4074-4081, 2019

Validation of magnetic resonance imaging-based automatic high-grade glioma segmentation accuracy via ^{11}C-methionine positron emission tomography

TOMOHIKO OZAKI[1], MANABU KINOSHITA[1], HIDEYUKI ARITA[2], NAOKI KAGAWA[2], YASUNORI FUJIMOTO[2], YONEHIRO KANEMURA[3,4], MIO SAKAI[5], YOSHIYUKI WATANABE[6], KATSUYUKI NAKANISHI[5], EKU SHIMOSEGAWA[7], JUN HATAZAWA[7] and HARUHIKO KISHIMA[2]

[1]Department of Neurosurgery, Osaka International Cancer Institute, Osaka 5418567; [2]Department of Neurosurgery, Osaka University Graduate School of Medicine, Suita, Osaka 5650871; [3]Department of Biomedical Research and Innovation, Institute for Clinical Research; [4]Department of Neurosurgery, Osaka National Hospital, National Hospital Organization, Osaka 5400006; [5]Department of Radiology, Osaka International Cancer Institute, Osaka 5418567; Departments of [6]Radiology and [7]Nuclear Medicine and Tracer Kinetics, Osaka University Graduate School of Medicine, Suita, Osaka 5650871, Japan

Received April 10, 2019; Accepted June 28, 2019

DOI: 10.3892/ol.2019.10734

Abstract. Brain Tumor Image Analysis (BraTumIA) is a fully automated segmentation tool dedicated to detecting brain tumors imaged by magnetic resonance imaging (MRI). BraTumIA has recently been applied to several clinical investigations; however, the validity of this novel method has not yet been fully examined. The present study was conducted to validate the quality of tumor segmentation with BraTumIA in comparison with results from ^{11}C-methionine positron emission tomography (MET-PET). A total of 45 consecutive newly diagnosed high-grade gliomas imaged by MRI and MET-PET were analyzed. Automatic tumor segmentation was conducted by BraTumIA and the resulting segmentation images were registered to MET-PET. Three-dimensional conformal association between these two modalities was calculated, considering MET-PET as the gold standard. High underestimation and overestimation errors were observed in tumor segmentation calculated by BraTumIA compared with MET-PET. Furthermore, when the tumor/normal ratio threshold was set at 1.3 from MET-PET, the BraTumIA false-positive fraction was ~0.4 and the false-negative fraction was 0.9. By tightening this threshold to 2.0, the BraTumIA false-positive fraction was 0.6 and the false-negative fraction was 0.6. Following comparison of segmentation performance with BraTumIA with regard to glioblastoma (GBM) and World Health Organization (WHO) grade III glioma, GBM exhibited better segmentation compared with WHO grade III glioma. Although BraTumIA may be able to detect enhanced tumors, non-enhancing tumors and necrosis, the spatial concordance rate with MET-PET was relatively low. Careful interpretation is therefore required when using this technique.

Correspondence to: Dr Manabu Kinoshita, Department of Neurosurgery, Osaka International Cancer Institute, 3-1-69 Otemae, Chuo, Osaka 5418567, Japan
E-mail: mail@manabukinoshita.com

Key words: malignant glioma, ^{11}C-methionine positron emission tomography, magnetic resonance imaging, automatic segmentation

Introduction

The overall age-adjusted incidence rates for all gliomas and glioblastoma range from 4.67 to 5.73 and 0.59 to 3.69 per 100,000 individuals, respectively across the United States, Georgia, Australia, Korea, England, Greece and Finland (1-7). The overall survival of patients with malignant glioma has slightly improved with the aid of radiotherapy, chemotherapy (8), tumor-treating fields (9) and advanced surgical techniques, including fluorescence-guided surgery with 5-aminolevulinic acid (10). However, the prognosis remains very poor, and the median overall survival time of patients with glioblastoma (GBM) is ~20 months (9). A more extensive surgical resection has been suggested to be associated with longer life expectancy in patients with malignant gliomas (11,12). However, malignant glioma presents with highly invasive characteristics, including subpial spread, perineural satellitosis, perivascular satellitosis and invasion along the white matter tracts (13), which prevent precise determination of the extent of tumor cell infiltration by magnetic resonance imaging (MRI) and therefore potentially contributes to poor local control of the lesion (14,15). The precise determination of the tumor cell infiltration extend has therefore become crucial.

Current strategies for treatment of glioma rely mostly on neuroimaging techniques, including MRI and computed tomography, in patients undergoing surgery and radiotherapy, and are used to identify regions where tumor cells exist. Sites of blood-brain barrier disruption on contrast-enhanced

T1-weighted (T1w) images are used as surrogate markers for active tumor regions; however, tumor cells can exist beyond the identified regions (16). Furthermore, it has been demonstrated that T2-weighted (T2w) hyperintense regions can contain tumors (17,18), whereas Susheela *et al* (19) reported a case of a high grade glioma which was present beyond the MRI defined edema region, and was demonstrated using ^{11}C-methionine positron emission tomography (MET-PET) (19). A single MRI sequence may therefore be insufficient to identify tumor regions.

Porz *et al* (20) evaluated the reliability of a fully automated segmentation tool dedicated to brain tumors known as Brain Tumor Image Analysis (BraTumIA) (20). The results demonstrated that the user only has to load the original stacks from the Digital Imaging and Communications in Medicine (DICOM) of the four relevant MRI modalities, including T1w, contrast-enhanced T1w, T2w and fluid-attenuated inversion recovery (FLAIR) images. The software subsequently classifies GBM into seven sub-compartments, including cerebrospinal fluid (CSF), gray matter, white matter, necrosis, edema, non-enhancing tumor and enhancing tumor. This tool, validated by the 'SmartBrush' semi-automatic user-guided and FDA-approved segmentation technique and human experts, has been reported to provide accurate, cross-sectional, diameter-based assessments of tumor extent and automated volume measurement of GBM (20). BraTumIA could also detect additional non-enhancing tumor regions that had been obscured by the semi-automatic segmentation tool in 16 out of 19 cases (21), which suggests the capability of BraTumIA to outperform semi-automatic segmentation tools. However, validating the presence of tumor cells in BraTumIA-labeled non-enhancing tumor regions remains necessary.

When attempting to understand the extent of brain tumor cells invading into the brain parenchyma, MET-PET is more effective than MRI (22-24). Kracht (23) reported an 87% sensitivity and 89% specificity for detecting tumor tissue at a threshold of 1.3-fold MET-PET uptake relative to normal brain tissue. Kinoshita *et al* (24) also demonstrated that MET-PET is positively correlated with glioma cell density (Fig. S1) (24). The present study aimed to validate the quality of tumor segmentation using BraTumIA compared with that using MET-PET.

Materials and methods

Patient selection. Data from 45 consecutive patients with newly diagnosed and histologically confirmed grade III and IV gliomas [according to the World Health Organization (WHO) 2007 Classification of Tumors of the Central Nervous System (25) were collected. Patients >18 years old, underwent MRI and MET-PET as preoperative examinations between May 2010 and March 2017 at the Osaka University Hospital and Osaka International Cancer Institution (Osaka, Japan). The exclusion criteria was incomplete image acquisition or previous cranial neurosurgery. Patients included in the present study underwent standard imaging protocols. No additional new procedures were applied for the purpose of this study. Written informed consent was obtained from each patient or their guardian prior to enrollment. This study was approved by the Clinical Research Committees of Osaka University Hospital and Osaka International Cancer Institution. Patient characteristics are provided in Table I.

MRI. All patients underwent T1w imaging with and without gadolinium enhancement, (undiluted and slowly injected into the vein of the arm). T2w and FLAIR imaging. A total of 5 cases were scanned using a 1.5-T MR scanner, whereas 40 cases were scanned using a 3.0-T scanner dependent on which hospital the scan was performed at.

PET. PET studies were performed using an Eminence-G system (Shimadzu Corporation). MET was synthesized according to the method described by Hatakeyama *et al* (26) and injected intravenously in patients at a dose of 3 MBq/kg body weight. Tracer accumulation was recorded for 12 min in 59 or 99 transaxial sections over the entire brain. Summed activity from 20 to 32 min following tracer injection was used for image reconstruction. Images were stored in 256x256x59 or 99 anisotropic voxels, with each voxel being 1x1x2.6 mm.

Automated segmentation. Automatic segmentations were performed using BraTumIA software version 2.0 (http://www.istb.unibe.ch/content/research/medical_image_analysis/software/index_eng.html) (20). Once the original DICOM stacks of the four MRI sequences (T1w with and without gadolinium enhancement, T2w and FLAIR images) were loaded, the software automatically distinguished the seven types of brain tissue, namely CSF, gray matter, white matter, necrosis, edema, non-enhancing tumor and enhancing tumor (Fig. 1).

Image fusion and registration. MET-PET and classification of MRI results by BraTumIA were obtained, and images were registered using the Vinci image-analyzing version 4 (Max-Planck Institute for Neurological Research; http://www.nf.mpg.de/vinci/). A normalized mutual information algorithm was used for image registration, and MET-PET was resliced into MR images, which enabled voxel-by-voxel analysis of different imaging modalities.

Data processing and region segmentation accuracy measures. Data sets were exported to in-house software written in MATLAB R2016b (MathWorks, Inc.) for further analysis. For the tumor-to-normal tissue ratio (T/Nr) of MET-PET, the standardized uptake value of the contralateral tumor-unaffected gray matter in the axial plane of the cortex was averaged, and the derived value was used to normalize the standardized uptake value in a voxel-wise manner, enabling calculation of T/Nr within the voxel-of-interest. Regions detected by BraTumIA exhibiting the presence of tumor were labeled as A + B, where A is the area identified as tumor exclusively by BraTumIA and B is the area identified as tumor by BraTumIA and MET-PET (Fig. 1). In addition, regions of high accumulation on MET-PET were labeled as B + C, where C is the area identified as tumor exclusively by MET-PET and B is the area identified as tumor by BraTumIA and MET-PET. The BraTumIA false-positive fraction was defined as A/(A + B) and the BraTumIA false-negative fraction was defined as C/(B + C).

Cell density. Kinoshita *et al* (24) reported that T/Nr from MET-PET is positively correlated with cell density in high-grade glioma as determined by liner regression analysis

Table I. Clinical characteristics of patients.

Characteristics	WHO grade III			WHO grade IV	Total
	Anaplastic astrocytoma	Anaplastic oligoastrocytoma	Anaplastic oligodendroglioma	Glioblastoma	
Patients, n	11	7	1	26	45
Sex, n (%)					
Male	8 (72.7)	5 (71.4)	1 (100)	14 (53.8)	28 (62.2)
Female	3 (27.3)	2 (28.6)	0 (0)	12 (46.2)	17 (37.8)
Mean age ± SD, years	58.9±16.6	59.4±21.3	35	59±14.4	58.5±15.9
Scanning technique, n					
Scanned in 3T	10	5	1	24	40
Scanned in 1.5T	1	2	0	2	5

WHO, World Health Organization; SD, standard deviation.

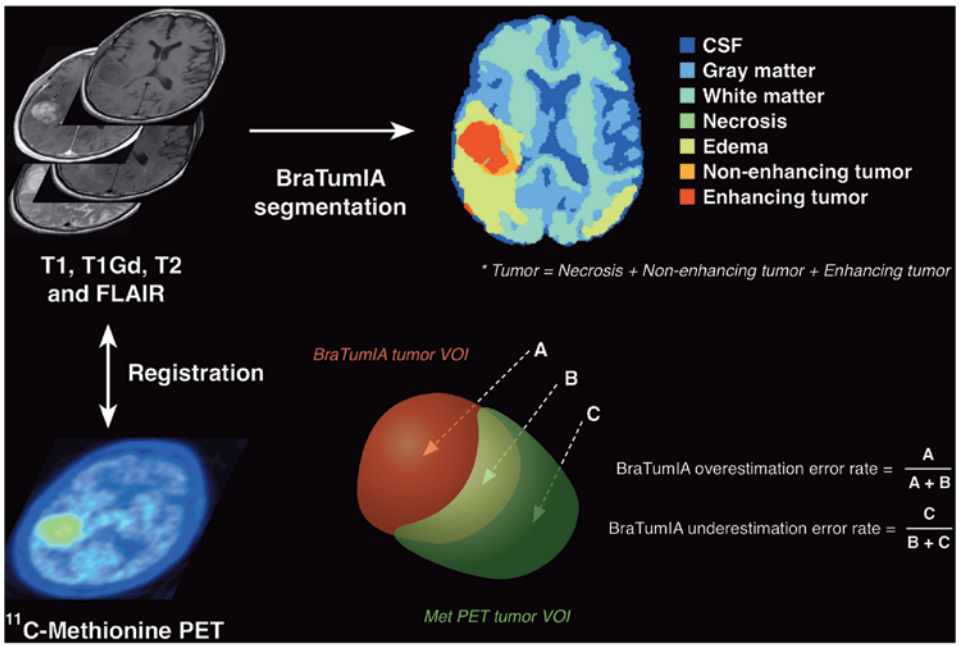

Figure 1. Analytical workflow of the present study. All images including 4 MR imaging sequences and ^{11}C-methionine PET were co-registered into a common space using a normalized mutual information algorithm to enable voxel-by-voxel analysis. Subsequently, all MR images were sent to BraTumIA for automatic region segmentation. Tumor regions were separately segmented in the common space by MET-PET using various cut-off thresholds. Region segmentation accuracy of BraTumIA was calculated considering MET-PET based segmentation as the gold standard. The BraTumIA false-positive fraction was defined as A/(A + B), and the BraTumIA false-negative fraction was defined as C/(B + C), where A represents the volume of the region segmented by BraTumIA but outside the MET-PET segmented region, B represents the volume of the region segmented by both BraTumIA and MET-PET, and C represents the volume of the region segmented by MET-PET but outside the BraTumIA segmented region. Values are reported as ratios of either A/(A + B) or C/(B + C), referred to as the false-positive and false-negative fractions, respectively. BraTumIA, Brain Tumor Image Analysis; CSF, cerebrospinal fluid; FLAIR, fluid-attenuated inversion recovery; Gd, gadolinium; MET, ^{11}C-methionine; MR, magnetic resonance; PET, positron emission tomography; VOI, voxel of interest.

using Pearson's correlation analysis (Fig. S1). Cell density data in Figs. 2-4 were obtained from Fig. S1.

Statistical analysis. Statistical analysis was performed using JMP version 11 software (SAS Institute, Inc.). Data are presented as the mean ± standard deviation (SD). The significance of differences between groups was examined using Student's t-test or one-way analysis of variance followed by the Tukey-Kramer post hoc test. Liner regression analysis using Pearson's correlation analysis was used to assess tumor cell density and MET-PET uptake. $P<0.05$ was considered to indicate a statistically significant difference.

Results

Patient population. The mean age of the patients at the time of pre-operative imaging was 58.5±15.9 years (range, 29-88 years). The 45 patients were comprised of 28 males and

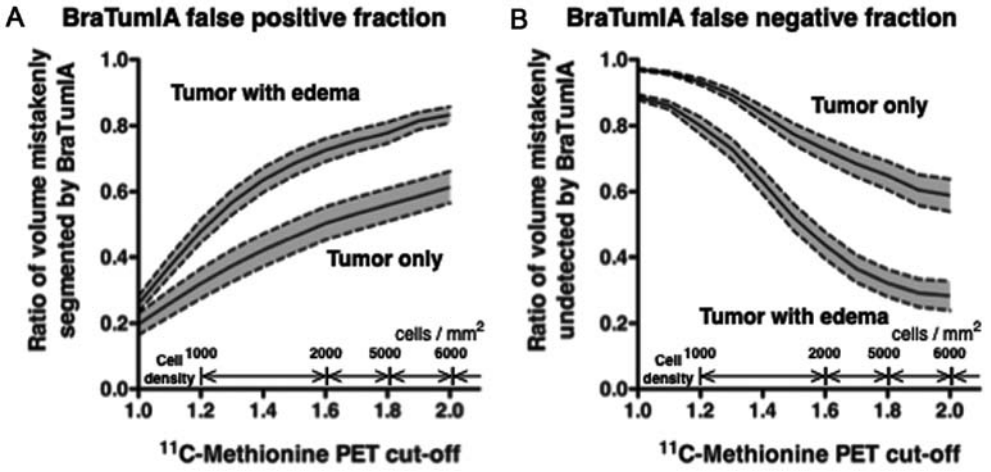

Figure 2. Concordance rate for the region of tumor existence as defined by BraTumIA with the region of high MET accumulation on PET. (A) False-positive fraction of the region of tumor existence and the region of tumor with edema as defined by BraTumIA validated with the region of high MET accumulation on PET. (B) False-negative fraction of the region of tumor existence and the region of tumor with edema as defined by BraTumIA validated with the region of high MET accumulation on PET. Data are presented as the mean ± standard deviation. The trend line was drawn by connecting the analyzed data by 0.1 increments in the T/Nr of MET accumulation on PET. BraTumIA, Brain Tumor Image Analysis; MET, ^{11}C-methionine; PET, positron emission tomography; T/Nr, tumor-to-normal tissue ratio.

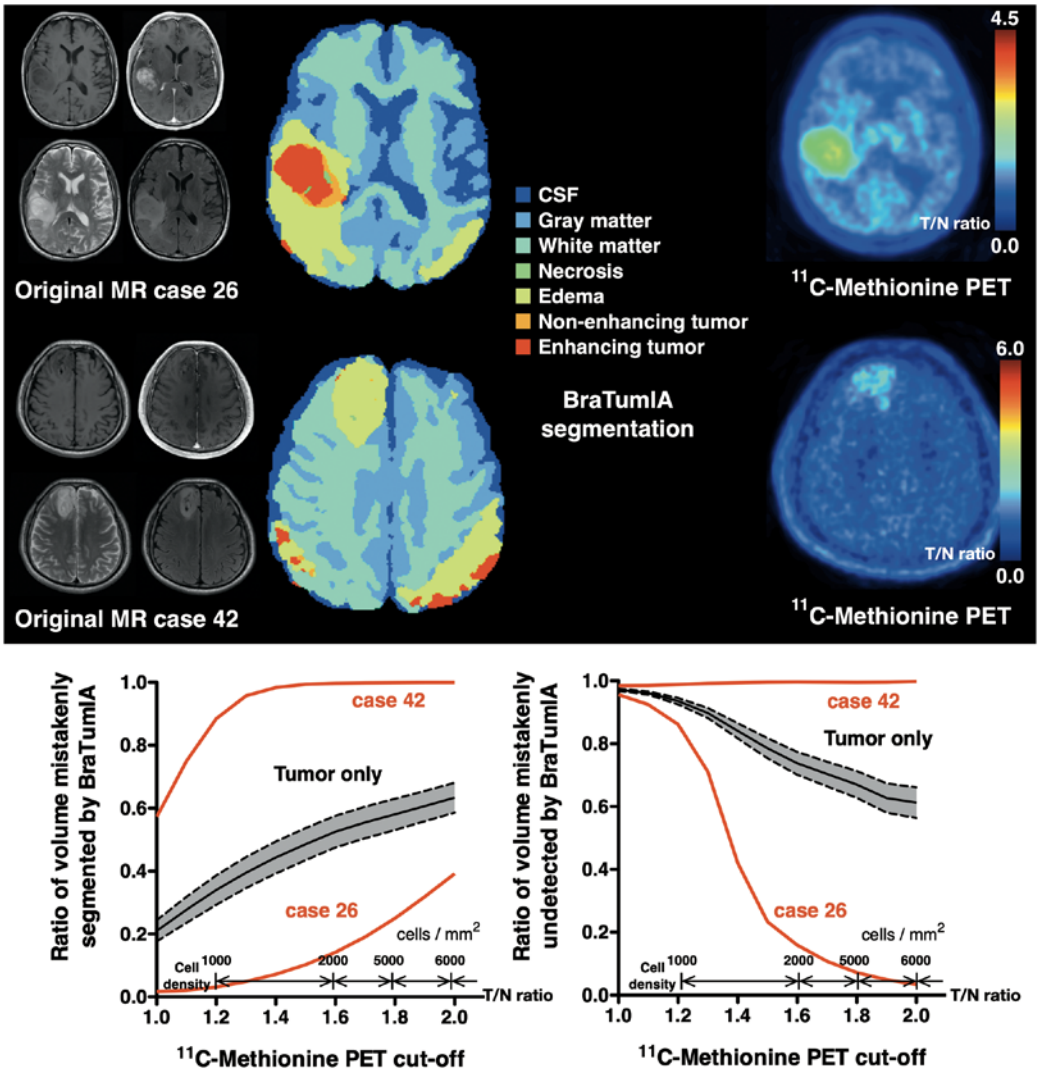

Figure 3. Cases in which the region of tumor existence on BraTumIA and the region of high accumulation on MET-PET showed good and poor correlations. The black curved line represents the mean ± standard deviation of all cases in the present study. The red curved line represents this case. The trend line was drawn by connecting the analyzed data by 0.1 increments in the T/Nr of MET accumulation on PET. BraTumIA, Brain Tumor Image Analysis; CSF, cerebrospinal fluid; MET, ^{11}C-methionine; MR, magnetic resonance; PET, positron emission tomography; T/Nr, tumor-to-normal tissue ratio.

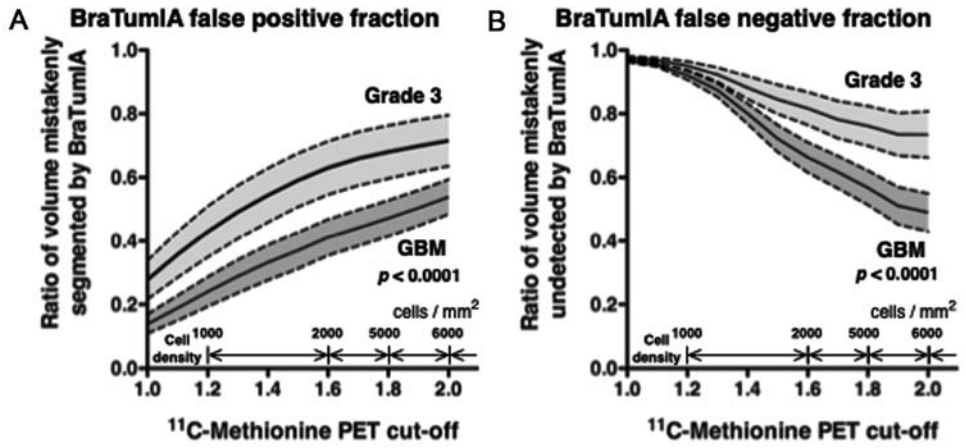

Figure 4. Concordance rate of the region of tumor existence as defined by BraTumIA with the region of high accumulation of MET accumulation on PET comparing World Health Organization grade III and GBM. (A) False-positive fraction of the region of tumor existence and the region of edema as defined by BraTumIA validated with the region of high MET accumulation on PET. (B) False-negative fraction of the region of tumor existence and the region of tumor with edema as defined by BraTumIA validated with the region of high MET accumulation on PET. Data represent the mean ± standard deviation. The trend line was drawn by connecting the analyzed data by 0.1 increments in the T/Nr of MET accumulation on PET. BraTumIA, Brain Tumor Image Analysis; GBM, glioblastoma; MET, ^{11}C-methionine; PET, positron emission tomography.

17 females. GBM was identified in 26 patients. All patients were histopathologically diagnosed according to the WHO 2007 Classification of Tumors of the Central Nervous System.

Brain segmentation by BraTumIA. T/Nr values for necrosis, non-enhancing tumor and enhancing tumor were significantly higher compared with those for other segments (P<0.001). No significant differences in T/Nr were identified between necrosis, non-enhancing tumor and enhancing tumor (Fig. 5). These observations were true for analyses of Grade III glioma and GBM and when confined to only GBM. Notably, significant overlaps were observed between segments 4-7 (necrosis, edema, non-enhancing tumor and enhancing tumor) with respect to MET-PET T/Nr.

Tumor distributions with BraTumIA and MET-PET. Porz *et al* (20) defined complete tumor volume as areas encompassing necrosis (segment 4), non-enhancing tumor (segment 6) and enhancing tumor (segment 7). Segments 4+6+7 were therefore initially defined as the region of tumor presence on BraTumIA (region A + B). When T/Nr threshold was set at 1.3, the BraTumIA false-positive fraction was ~0.4 and the false-negative fraction was 0.9. This threshold was close to the threshold proposed by Kracht (23) that discriminates glioma tissues from normal brain tissues. When a T/Nr threshold of 2.0 was used, the false-positive fraction with BraTumIA increased to 0.6, whereas the false-negative fraction with BraTumIA decreased to 0.6 (Fig. 2).

Subsequently, the effect of the edema region on BraTumIA was investigated. Segments 4+5+6+7 were defined as the region of tumor existence for this purpose (region A + B). When the T/Nr threshold was set to 1.3, the false-positive fraction with BraTumIA was ~0.6 and the false-negative fraction was 0.7. When a T/Nr threshold of 2.0 was used, the false-positive fraction with BraTumIA increased to 0.8, whereas the false-negative fraction decreased to 0.3 (Fig. 2).

Fig. 3 illustrates a patient case (original MR case no. 26) in which the region of tumor existence on BraTumIA (segment 4+6+7) and the high accumulation region on MET-PET matched well. The BraTumIA false-positive fraction was <0.1 when the T/Nr threshold was 1.3, and was still ~0.4 even with a T/Nr threshold of 2.0. Furthermore, the BraTumIA false-negative fraction was ~0.6 when the T/Nr threshold was 1.3 and decreased to <0.1 when the T/Nr threshold was increased to 2.0. Conversely, Fig. 3 illustrates a patient case (original MR case no. 42) in which the region of tumor existence on BraTumIA (segment 4+6+7) and the high-accumulation region on MET-PET showed a large discrepancy.

With regards to GBM, when the T/Nr threshold was set to 1.3, the BraTumIA false-positive fraction was ~0.3 and the false-negative fraction was ~0.9. When a T/Nr threshold of 2.0 was used, these errors were both ~0.5 (Fig. 4). For grade III glioma, when the T/Nr threshold was 1.3, the BraTumIA false-positive fraction was ~0.5 and the false-negative fraction was ~0.95. When a T/Nr threshold of 2.0 was used, these errors were both ~0.7 (Fig. 4).

Discussion

The present study attempted to validate BraTumIA as a method for GBM diagnosis by comparing it to the gold standard MET-PET. To the best of our knowledge, this type of validation has not yet been performed. The results demonstrated that BraTumIA presented a significantly higher T/Nr in the enhancing tumor region, non-enhancing tumor region and necrosis region compared with other regions. These regions were defined as 'the complete tumor volume' by Porz *et al* (20) and the results from this study confirmed that BraTumIA could recognize regions of tumor existence within the brain. In particular, T/Nr values in necrotic lesions were significantly high, suggesting limitations to the tumor segmentation capability of BraTumIA. Kracht (23) described a mean ± SD threshold of relative MET uptake of 1.96±0.47 for solid regions and 1.74±0.52 for tumor-infiltrated regions in GBM (23). When considering enhancing tumor regions on BraTumIA as solid regions and non-enhancing tumor regions as infiltrated regions, the results

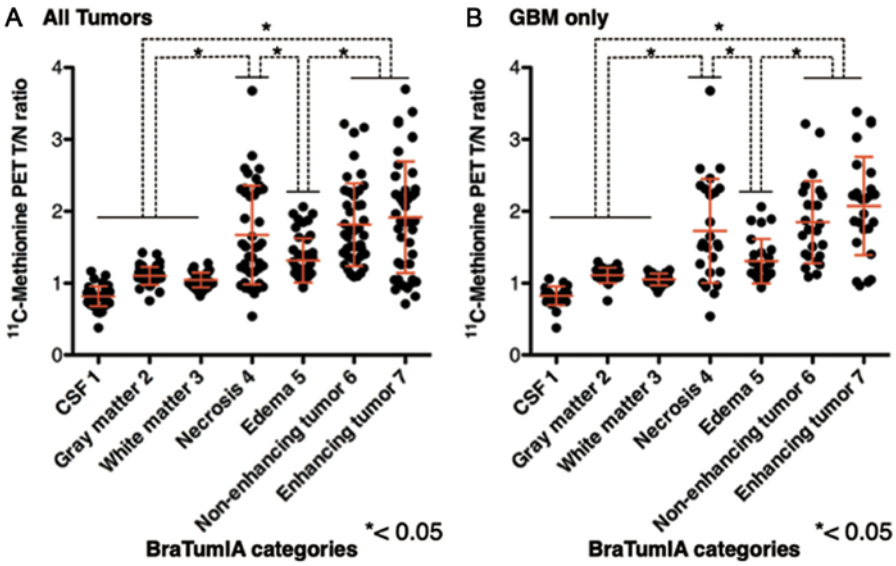

Figure 5. ^{11}C-Methionine PET T/Nr for each region segmented by BraTumIA. Individual data points with mean ± standard deviation (marked by red lines) for ^{11}C-methionine PET T/Nr in each region segmented by BraTumIA are presented for both analyses using (A) all the datasets and (B) confined to glioblastoma alone. *P<0.05. Statistical analysis was performed using one-way analysis of variance followed by Tukey-Kramer post hoc test. BraTumIA, Brain Tumor Image Analysis; CSF, cerebrospinal fluid; PET, positron emission tomography; T/Nr, tumor-to-normal tissue ratio.

from the present study were comparable to those described by Kracht (23). Regions of necrosis exhibited lower T/Nr values compared with enhancing and non-enhancing tumor regions. Goldman *et al* (27) described anaplastic regions in high-grade gliomas as having higher MET uptake compared with regions without histological signs of anaplasia, and further reported that the presence of necrosis in anaplastic samples caused decreased MET uptake. In addition, Goldman *et al* (27) reported that the mean ± SD T/Nr of anaplastic samples with no necrosis was 2.72±0.90, whereas it was 1.84±1.10 and 1.20±0.36 for regions of focal necrosis and extensive necrosis, respectively. These results are comparable to the results obtained in the present study. T/Nr in regions of edema tended to be higher than in CSF, gray matter or white matter, although the difference was not significant. Kinoshita *et al* (24) reported a positive correlation of MET-PET with glioma cell density. Subsequently, regions of edema segmented by BraTumIA may have contained active tumor cells detected by MET-PET. Furthermore, a significant overlap was observed between segments 4-7 (necrosis, edema, non-enhancing tumor and enhancing tumor) with respect to the MET-PET T/Nr. Although BraTumIA could identify four out of the seven segments or brain regions (CSF, gray matter, white matter, enhancing tumor), identification of the remaining three segments (necrosis, edema and non-enhancing tumor) was more problematic. For example, the MET-PET T/Nr of the necrosis region significantly overlapped with that of the enhancing tumor, suggesting that the algorithm over-segmented regions of necrosis.

In the present study, the complete tumor region was defined as regions encompassing necrosis, non-enhancing tumor and enhancing tumor on BraTumIA, similarly to the method described by Porz *et al* (20). Adding edema regions to regions of tumor existence decreased the false-negative fraction for BraTumIA, but increased the false-positive fraction, as predicted. Overall, although BraTumIA may be able to distinguish tumor and other regions, including regions of edema, the spatial concordance rate with MET-PET remained unsatisfactory. Miwa *et al* (28) reported that only 58.6% of MET uptake area is included within the gadolinium-enhanced area in GBM. Similarly, Grosu *et al* (29) reported that only 31.6% of the MET uptake area is included within the gadolinium-enhanced area, and that 56.5% of the MET uptake area is included within the area of T2 hyperintensity in high-grade gliomas. Furthermore, a recent study demonstrated that the diagnostic accuracy of MET-PET is better than that of conventional anatomical MR in high-grade glioma, which is similar to the results from the current study (30) and suggests that reliance on MRI alone for glioma segmentation may require caution. Furthermore, BraTumIA had limited lesion-segmentation capability for non-enhancing lesions. In addition, the results demonstrated that a visually well-recognized non-enhancing lesion in the right frontal lobe was mis-segmented as 'edema', which was likely caused by the fact that no information on tumor enhancement by contrast agents is available for BraTumIA.

When comparing GBM and WHO grade III gliomas, BraTumIA performed significantly better in accuracy for GBM than for grade III tumors. One possible reason for this result may be associated with the gadolinium-enhancing characteristics of the tumor, since contrast enhancement of the tumor is known to be associated with glioma grade (19,31). Porz *et al* (20) demonstrated that BraTumIA could detect the contrast-enhancing tumor region with high accuracy. This result raised some concerns regarding the use of BraTumIA in non-GBM gliomas, as the segmentation accuracy may be lower than that expected by researchers.

BraTumIA has been used to estimate the extent of resection and residual tumor volume in patients with GBM (32), and has been reported to be suitable for the follow-up of GBM progression (33). Dextraze *et al* (34) reported that MRI imaging analyzed by BraTumIA were associated with signaling pathway activities and survival in GBM (34). Although these examples show the potential of BraTumIA to analyze clinical

data from patients with gliomas, the results from the present study indicated that caution is warranted when fully relying on this technique, and that the results obtained using this novel technology should be carefully interpreted.

Some limitations should be addressed for the current study. MET-PET was considered as the gold standard when assessing the accuracy of lesion extraction using BraTumIA. Although MET-PET has frequently been described as a useful tool to detect tumor cell infiltration beyond the primary enhancing lesion (23,24,35-37), the lesion presentation is not mechanistically or functionally linked with MRI. As a result, the accuracy of lesion segmentation with BraTumIA presented in the current study depended greatly on the cut-off values adopted from MET-PET.

In conclusion, BraTumIA brain tumor auto-segmentation software has been validated by MET-PET. Although the results from the present study indicated that BraTumIA may be able to detect enhancing tumors, non-enhancing tumors and necrosis, the rate of spatial concordance with MET-PET was relatively low. Careful interpretation is therefore required when using this technique.

Acknowledgements

The authors would like to thank Ms. Ai Takada (Institute for Clinical Research, Osaka National Hospital, National Hospital Organizatio) and Ms. Mariko Kakinoki (Department of Neurosurgery, Osaka International Cancer Institute) for their support in conducting this research.

Funding

The present study was supported by JSPS KAKENHI (grants nos. 16K10778 and 17H05308), the Osaka Medical Research Foundation for Intractable Diseases (funding information not applicable), the Uehara Memorial Foundation (funding information not applicable) and the MSD Life Science Foundation (funding information not applicable).

Availability of data and materials

The datasets used and/or analyzed during the present study are available from the corresponding author on reasonable request.

Authors' contributions

TO and MK wrote the manuscript and collected the data. TO, MK and HK designed the study and analyzed the data. HA, NK, YF, YK collected the tumor samples. MS, YW, KN collected the MRI images. ES and JH collected the MET-PET images. All authors read and approved the final manuscript.

Ethics approval and consent to participate

The present study was approved by the Clinical Research Committees of Osaka University Hospital and Osaka International Cancer Institution (Osaka, Japan). Signed informed consent was obtained from the patients or their guardians for participation in the present study.

Patient consent for publication

Not applicable.

Competing interests

The authors declare that they have no competing interests.

References

1. Ostrom QT, Gittleman H, Farah P, Ondracek A, Chen Y, Wolinsky Y, Stroup NE, Kruchko C and Barnholtz-Sloan JS: CBTRUS statistical report: Primary brain and central nervous system tumors diagnosed in the United States in 2006-2010. Neuro Oncol 15 (Suppl 2): ii1-ii56, 2013.
2. Gigineishvili D, Shengelia N, Shalashvili G, Rohrmann S, Tsiskaridze A and Shakarishvili R: Primary brain tumour epidemiology in Georgia: First-year results of a population-based study. J Neurooncol 112: 241-246, 2013.
3. Dobes M, Khurana VG, Shadbolt B, Jain S, Smith SF, Smee R, Dexter M and Cook R: Increasing incidence of glioblastoma multiforme and meningioma, and decreasing incidence of Schwannoma (2000-2008): Findings of a multicenter Australian study. Surg Neurol Int 2: 176, 2011.
4. Gousias K, Markou M, Voulgaris S, Goussia A, Voulgari P, Bai M, Polyzoidis K, Kyritsis A and Alamanos Y: Descriptive epidemiology of cerebral gliomas in northwest Greece and study of potential predisposing factors, 2005-2007. Neuroepidemiology 33: 89-95, 2009.
5. Larjavaara S, Mäntylä R, Salminen T, Haapasalo H, Raitanen J, Jääskeläinen J and Auvinen A: Incidence of gliomas by anatomic location. Neuro Oncol 9: 319-325, 2007.
6. Arora RS, Alston RD, Eden TO, Estlin EJ, Moran A and Birch JM: Age-incidence patterns of primary CNS tumors in children, adolescents, and adults in England. Neuro Oncol 11: 403-413, 2009.
7. Lee CH, Jung KW, Yoo H, Park S and Lee SH: Epidemiology of primary brain and central nervous system tumors in Korea. J Korean Neurosurg Soc 48: 145-152, 2010.
8. Stupp R, Mason WP, van den Bent MJ, Weller M, Fisher B, Taphoorn MJ, Belanger K, Brandes AA, Marosi C, Bogdahn U, *et al*: Radiotherapy plus concomitant and adjuvant temozolomide for glioblastoma. N Engl J Med 352: 987-996, 2005.
9. Stupp R, Taillibert S, Kanner AA, Kesari S, Steinberg DM, Toms SA, Taylor LP, Lieberman F, Silvani A, Fink KL, *et al*: Maintenance therapy with tumor-treating fields plus temozolomide vs temozolomide alone for glioblastoma: A randomized clinical trial. JAMA 314: 2535-2543, 2015.
10. Stummer W, Pichlmeier U, Meinel T, Wiestler OD, Zanella F, Reulen HJ and ALA-Glioma Study Group: Fluorescence-guided surgery with 5-aminolevulinic acid for resection of malignant glioma: A randomised controlled multicentre phase III trial. Lancet Oncol 7: 392-401, 2006.
11. Sanai N and Berger MS: Glioma extent of resection and its impact on patient outcome. Neurosurgery 62: 753-764, 2008.
12. Devaux BC, O'Fallon JR and Kelly PJ: Resection, biopsy, and survival in malignant glial neoplasms: A retrospective study of clinical parameters, therapy, and outcome. J Neurosurg 78: 767-775, 1993.
13. Zagzag D, Esencay M, Mendez O, Yee H, Smirnova I, Huang Y, Chiriboga L, Lukyanov E, Liu M and Newcomb EW: Hypoxia- and vascular endothelial growth factor-induced stromal cell-derived factor-1alpha/CXCR4 expression in glioblastomas: One plausible explanation of Scherer's structures. Am J Pathol 173: 545-560, 2008.
14. Kotrotsou A, Elakkad A, Sun J, Thomas GA, Yang D, Abrol S, Wei W, Weinberg JS, Bakhtiari AS, Kircher MF, *et al*: Multi-center study finds postoperative residual non-enhancing component of glioblastoma as a new determinant of patient outcome. J Neurooncol 139: 125-133, 2018.
15. Ellingson BM, Abrey LE, Nelson SJ, Kaufmann TJ, Garcia J, Chinot O, Saran F, Nishikawa R, Henriksson R, Mason WP, *et al*: Validation of postoperative residual contrast-enhancing tumor volume as an independent prognostic factor for overall survival in newly diagnosed glioblastoma. Neuro Oncol 20: 1240-1250, 2018.
16. Pirzkall A, McKnight TR, Graves EE, Carol MP, Sneed PK, Wara WW, Nelson SJ, Verhey LJ and Larson DA: MR-spectroscopy guided target delineation for high-grade gliomas. Int J Radiat Oncol Biol Phys 50: 915-928, 2001.

17. Daumas-Duport C, Monsaigneon V, Blond S, Munari C, Musolino A, Chodkiewicz JP and Missir O: Serial stereotactic biopsies and CT scan in gliomas: Correlative study in 100 astrocytomas, oligo-astrocytomas and oligodendrocytomas. J Neurooncol 4: 317-328, 1987.
18. Kelly PJ, Daumas-Duport C, Kispert DB, Kall BA, Scheithauer BW and Illig JJ: Imaging-based stereotaxic serial biopsies in untreated intracranial glial neoplasms. J Neurosurg 66: 865-874, 1987.
19. Susheela SP, Revannasiddaiah S, Madhusudhan N and Bijjawara M: The demonstration of extension of high-grade glioma beyond magnetic resonance imaging defined edema by the use of (11) C-methionine positron emission tomography. J Cancer Res Ther 9: 715-717, 2013.
20. Porz N, Bauer S, Pica A, Schucht P, Beck J, Verma RK, Slotboom J, Reyes M and Wiest R: Multi-modal glioblastoma segmentation: Man versus machine. PLoS One 9: e96873, 2014.
21. Porz N, Habegger S, Meier R, Verma R, Jilch A, Fichtner J, Knecht U, Radina C, Schucht P, Beck J, *et al*: Fully automated enhanced tumor compartmentalization: Man vs. machine reloaded. PLoS One 11: e0165302, 2016.
22. Herholz K, Hölzer T, Bauer B, Schröder R, Voges J, Ernestus RI, Mendoza G, Weber-Luxenburger G, Löttgen J, Thiel A, *et al*: 11C-methionine PET for differential diagnosis of low-grade gliomas. Neurology 50: 1316-1322, 1998.
23. Kracht LW, Miletic H, Busch S, Jacobs AH, Voges J, Hoevels M, Klein JC, Herholz K and Heiss WD: Delineation of brain tumor extent with [11C]L-methionine positron emission tomography: Local comparison with stereotactic histopathology. Clin Cancer Res 10: 7163-7170, 2004.
24. Kinoshita M, Arita H, Okita Y, Kagawa N, Kishima H, Hashimoto N, Tanaka H, Watanabe Y, Shimosegawa E, Hatazawa J, *et al*: Comparison of diffusion tensor imaging and ^{11}C-methionine positron emission tomography for reliable prediction of tumor cell density in gliomas. J Neurosurg 125: 1136-1142, 2016.
25. Louis DN, Ohgaki H, Wiestler OD, Cavenee WK, Burger PC, Jouvet A, Scheithauer BW and Kleihues P: The 2007 WHO classification of tumours of the central nervous system. Acta Neuropathol 114: 97-109, 2007.
26. Hatakeyama T, Kawai N, Nishiyama Y, Yamamoto Y, Sasakawa Y, Ichikawa T and Tamiya T: 11C-methionine (MET) and 18F-fluorothymidine (FLT) PET in patients with newly diagnosed glioma. Eur J Nucl Med Mol Imaging 35: 2009-2017, 2008.
27. Goldman S, Levivier M, Pirotte B, Brucher JM, Wikler D, Damhaut P, Dethy S, Brotchi J and Hildebrand J: Regional methionine and glucose uptake in high-grade gliomas: A comparative study on PET-guided stereotactic biopsy. J Nucl Med 38: 1459-1462, 1997.
28. Miwa K, Shinoda J, Yano H, Okumura A, Iwama T, Nakashima T and Sakai N: Discrepancy between lesion distributions on methionine PET and MR images in patients with glioblastoma multiforme: Insight from a PET and MR fusion image study. J Neurol Neurosurg Psychiatry 75: 1457-1462, 2004.
29. Grosu AL, Weber WA, Riedel E, Jeremic B, Nieder C, Franz M, Gumprecht H, Jaeger R, Schwaiger M and Molls M: L-(methyl-11C) methionine positron emission tomography for target delineation in resected high-grade gliomas before radiotherapy. Int J Radiat Oncol Biol Phys 63: 64-74, 2005.
30. Verburg N, Hoefnagels FWA, Barkhof F, Boellaard R, Goldman S, Guo J, Heimans JJ, Hoekstra OS, Jain R, Kinoshita M, *et al*: Diagnostic accuracy of neuroimaging to delineate diffuse gliomas within the brain: A meta-analysis. AJNR Am J Neuroradiol 38: 1884-1891, 2017.
31. Tynninen O, Aronen HJ, Ruhala M, Paetau A, Von Boguslawski K, Salonen O, Jääskeläinen J and Paavonen T: MRI enhancement and microvascular density in gliomas. Correlation with tumor cell proliferation. Invest Radiol 34: 427-434, 1999.
32. Meier R, Porz N, Knecht U, Loosli T, Schucht P, Beck J, Slotboom J, Wiest R and Reyes M: Automatic estimation of extent of resection and residual tumor volume of patients with glioblastoma. J Neurosurg 127: 798-806, 2017.
33. Meier R, Knecht U, Loosli T, Bauer S, Slotboom J, Wiest R and Reyes M: Clinical evaluation of a fully-automatic segmentation method for longitudinal brain tumor volumetry. Sci Rep 6: 23376, 2016.
34. Dextraze K, Saha A, Kim D, Narang S, Lehrer M, Rao A, Narang S, Rao D, Ahmed S, Madhugiri V, *et al*: Spatial habitats from multiparametric MR imaging are associated with signaling pathway activities and survival in glioblastoma. Oncotarget 8: 112992-113001, 2017.
35. Ullrich RT, Kracht L, Brunn A, Herholz K, Frommolt P, Miletic H, Deckert M, Heiss WD and Jacobs AH: Methyl-L-11C-methionine PET as a diagnostic marker for malignant progression in patients with glioma. J Nucl Med 50: 1962-1968, 2009.
36. Kinoshita M, Arita H, Goto T, Okita Y, Isohashi K, Watabe T, Kagawa N, Fujimoto Y, Kishima H, Shimosegawa E, *et al*: A novel PET index, 18F-FDG-11C-methionine uptake decoupling score, reflects glioma cell infiltration. J Nucl Med 53: 1701-1708, 2012.
37. Wu R, Watanabe Y, Arisawa A, Takahashi H, Tanaka H, Fujimoto Y, Watabe T, Isohashi K, Hatazawa J and Tomiyama N: Whole-tumor histogram analysis of the cerebral blood volume map: Tumor volume defined by 11C-methionine positron emission tomography image improves the diagnostic accuracy of cerebral glioma grading. Jpn J Radiol 35: 613-621, 2017.